ChemComm

RSC Publishing

COMMUNICATION

View Article Online
View Journal | View Issue

Cite this: *Chem. Commun.*, 2013, **49**, 10088

Received 17th June 2013,
Accepted 5th September 2013

DOI: 10.1039/c3cc44523b

www.rsc.org/chemcomm

Surfactant-free hydrothermal synthesis of sub-10 nm γ-Fe_2O_3–polymer porous composites with high catalytic activity for reduction of nitroarenes†

Xianmo Gu,[ab] Zhenhua Sun,*[b] Shuchang Wu,[b] Wei Qi,[b] Haihua Wang,[b] Xianzhu Xu*[a] and Dangsheng Su*[b]

Porous γ-Fe_2O_3–polymer composites were synthesized by a novel one-pot surfactant-free hydrothermal approach. The γ-Fe_2O_3–polymer composites consisting of 3.5 nm γ-Fe_2O_3 nanoparticles and porous polymers exhibited high catalytic activity and recycling performance in the reduction of nitroarenes.

Iron oxide nanoparticles have attracted considerable interest because of their potential for use in a wide range of applications, for example, ferrofluids, biomedical imaging, drug and gene delivery, energy storage devices, wastewater cleaning, and catalysis.[1–4] The physical and chemical properties of iron oxides are largely dependent on their structures, morphologies, and sizes.[5] To date, some studies have indicated that iron oxide nanoparticles of small size have excellent catalytic performance due to their large specific surface area.[6] Therefore, synthesis of sub-10 nm iron oxide nanoparticles with controllable structure and size has been developed in recent years.

Various wet chemical processes have been used to synthesize maghemite nanoparticles including precipitation, thermolysis by organic metallic composition and carbonyl composition.[7–9] Alivisatos *et al.* have successfully synthesized moderately monodispersed γ-Fe_2O_3 nanocrystals of 6–7 nm diameters by injecting solutions of cupferron complexes into long-chain amines at 300 °C.[7] During the process, high temperature and toxic organic solvents were used, which were detrimental for energy conservation and environmental protection. Cui *et al.* have reported a facile solvothermal synthesis of near monodispersed Fe_3O_4 nanoparticles on a gram scale.[8] Although this method was carried out at a low temperature, the synthesis needed a surfactant as a stabilizer. Therefore, it is very necessary to develop a facile method to synthesize sub-10 nm iron oxide nanoparticles in the non-toxic system under mild conditions. Meanwhile, the metal oxide–polymer composites have recently been receiving increasing attention in many applications ranging from catalysis, light emitting diodes, and solar energy cells.[10–12] The polymer not only served as a carrier of metal oxide particles, but also controlled the structures and morphology of metal oxide particles. So far, various approaches have been reported for the synthesis of metal oxide–polymer composites, but there are only a few methods reported for the one-pot synthesis of sub-10 nm metal oxide nanoparticle–polymer composites in an environmentally friendly system. Herein, we report a one-pot surfactant-free hydrothermal route to synthesize sub-10 nm γ-Fe_2O_3–polymer porous composites by the thermal decomposition of iron(III) acetylacetonate followed by the polymerization with formaldehyde under the alkaline conditions. Compared with previous reports, this method has the advantages of facileness, non-toxic and economical. More importantly, γ-Fe_2O_3 in the γ-Fe_2O_3–polymer composites was sub-10 nm in size and exhibited excellent catalytic activity and recycling performance in the reduction of nitrobenzene to aniline.

The γ-Fe_2O_3–polymer composites were obtained by the thermal decomposition of iron(III) acetylacetonate and formaldehyde under the basic conditions at 160 °C. The detailed experimental process is described in the ESI.† The reaction process is summarized in Scheme 1. Iron(III) acetylacetonate was first decomposed into an acetylacetonate anion and iron hydroxide under alkaline conditions when the temperature of the reaction system was raised to 160 °C. Then, the acetylacetonate anion reacted with formaldehyde to produce polymers. Meanwhile, iron hydroxide was converted into γ-Fe_2O_3 nanoparticles. Finally, γ-Fe_2O_3–polymer composites were

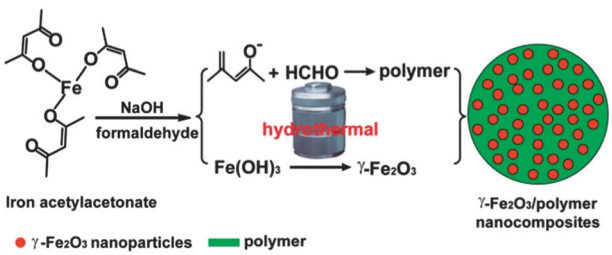

Scheme 1 The formation process of the γ-Fe_2O_3–polymer composites.

[a] *State Key Laboratory of Urban Water Resource and Environment, Harbin Institute of Technology, Harbin 150090, P. R. China. E-mail: xuxianzhu@hit.edu.cn; Fax: +86 451 86403625; Tel: +86 451 86403715*

[b] *Shenyang National Laboratory for Material Science, Institute of Metal Research, Chinese Academy of Sciences, 110016 Shenyang, P. R. China. E-mail: zhsun@imr.ac.cn, dangsheng@fhi-berlin.mpg.de; Fax: +86 24 83970019; Tel: +86 24 83978238*

† Electronic supplementary information (ESI) available: Experimental details, characterization, catalytic measurement, a table of synthetic parameters and catalytic activity, XRD, TEM and SEM images. See DOI: 10.1039/c3cc44523b

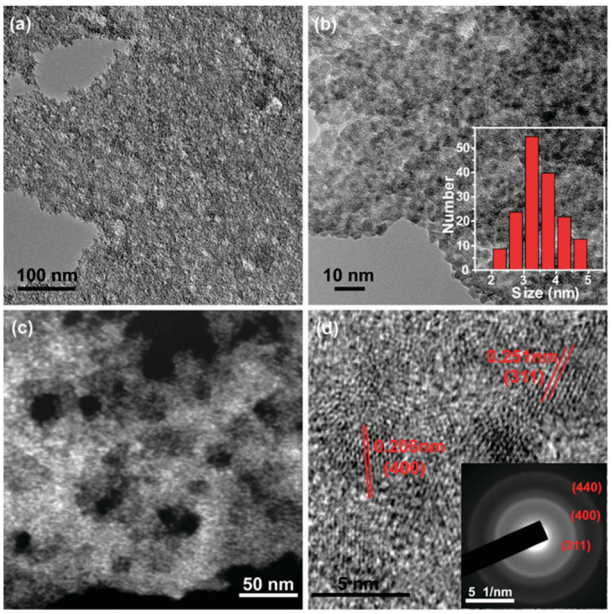

Fig. 1 TEM (a and b), HAADF-STEM (c) and HRTEM (d) images of the γ-Fe_2O_3–polymer composites. Insets in (b) and (d) show the size distribution and the SAED pattern of γ-Fe_2O_3 nanoparticles, respectively.

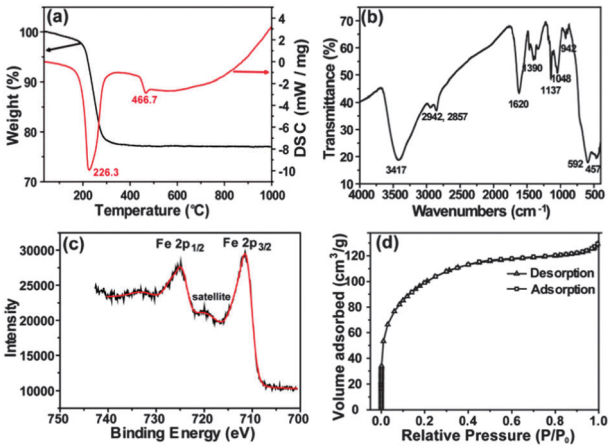

Fig. 2 TG-DSC curves (a), FT-IR spectrum (b), XPS spectrum (c) and N_2 adsorption isotherm (d) of the γ-Fe_2O_3–polymer composites.

formed after 4 hours. It was important to emphasize that the formation of polymers and γ-Fe_2O_3 nanoparticles occurred nearly simultaneously. Therefore, γ-Fe_2O_3 nanoparticles were uniformly dispersed in the polymers. In addition, the average size of γ-Fe_2O_3 nanoparticles is 3.5 nm and is uniformly distributed, due to the inhibition of the growth of the nanocrystals by the polymers.

The morphology and structure of as-synthesized γ-Fe_2O_3–polymer composites were characterized by transmission electron microscopy (TEM), high-angle annular dark-field scanning transmission-electron microscopy (HAADF-STEM), high-resolution TEM (HRTEM), selected-area electron diffraction (SAED) and X-ray diffraction (XRD). The TEM images (Fig. 1a and b) display that the γ-Fe_2O_3 nanoparticles are uniformly embedded in the polymers, similar to the lotus seeds in the lotus seedpod. The size of γ-Fe_2O_3 nanoparticles was measured based on the TEM image and the average size of γ-Fe_2O_3 nanoparticles is approximately 3.5 ± 0.7 nm (inset in Fig. 1b). Moreover, the HAADF-STEM image (Fig. 1c) further demonstrated the homogeneity of γ-Fe_2O_3 nanoparticles in the polymers. The HRTEM (Fig. 1d) displayed that *d*-spacings of adjacent fringes were 0.251 nm and 0.206 nm, corresponding to the (311) plane and the (400) plane of γ-Fe_2O_3 respectively. The SAED pattern of the composites had three visible diffraction rings, which are (311), (400), (440) planes of γ-Fe_2O_3 from the inside out (as shown in the inset in Fig. 1d). Furthermore, the XRD pattern of the γ-Fe_2O_3–polymer composites had two broad peaks due to the smaller size nanoparticles embedded in the polymers (Fig. S1, ESI†). In order to confirm the crystal phase of nanoparticles, the composites were calcined in air at 350 °C and 500 °C for 2 h, respectively. After calcination at 350 °C, most of the polymers were burned off, and the nanoparticles were mostly indexed as the maghemite crystal phase, which is in agreement with HRTEM and SAED data. However, the nanoparticles were transformed into hematite after calcination at 500 °C, because maghemite is thermally unstable.[13] Moreover, the room-temperature Mössbauer spectrum of the γ-Fe_2O_3–polymer composites (Fig. S2, ESI†) displayed doublet peaks with an isomer shift of 0.34 mm s^{-1} and quadrupolar splitting of 0.68 mm s^{-1}, which corresponded to γ-Fe_2O_3.[14]

TGA–DSC curves of γ-Fe_2O_3–polymer composites indicated possible polymer content and the phase transformation of γ-Fe_2O_3 at increasing temperature under an air atmosphere (Fig. 2a). The relatively large mass loss from 160 to 370 °C was about ~20.9%, which is attributed to the combustion of the polymer, and there is a large exothermic peak in the DSC curves, corresponding to the combustion of the polymer. Another small exothermic peak at 466.7 °C in the DSC curve is attributed to the transformation of the γ-Fe_2O_3 phase to the α-Fe_2O_3 phase.[13] Therefore, there is no obvious weight loss in the TGA curves at the corresponding temperature. Furthermore, there is no phase transformation peak observed in the DSC curve of the composites after calcination at 500 °C (Fig. S3, ESI†). Based on these results, iron oxide species can be indexed as γ-Fe_2O_3. In addition, the FTIR spectrum (Fig. 2b) exhibits the bonding state of carbon and iron. The peaks centered at 2942, 2857, 1471 and 1390 cm^{-1} can be assigned to the stretching and deformation vibration of C–H, respectively. A broad peak is observed at *ca.* 3417 cm^{-1}, which is assigned to OH stretching. The peak centered at 1620 cm^{-1} was ascribed to the stretching vibration of C═O.[15] In addition, the peaks at 592 cm^{-1} and 457 cm^{-1} were attributed to Fe–O stretching vibration.[16] X-ray photoelectron spectroscopy (XPS) analysis (Fig. 2c) was carried out to investigate the oxidation state of iron oxide nanoparticles encapsulated in the polymer. Two band energies of 724.9 and 711.5 eV are assigned to Fe $2p_{1/2}$ and Fe $2p_{3/2}$ of Fe^{3+}. The satellite peak situated at 719.5 eV is a major characteristic of Fe^{3+} in γ -Fe_2O_3.[17] The nitrogen sorption isotherm (Fig. 2d) is similar to the type I isotherm which has a pronounced slope at very low relative pressure, due to the filling of micropores.[18] Moreover, the BET surface area of the composites is about 369.5 m^2 g^{-1} and the pore diameter is 0.55 nm.

To investigate the influence of the polymer formation on the size of γ-Fe_2O_3 nanoparticles, a series of control experiments were conducted (Table S1, ESI†). When no formaldehyde was added, only γ-Fe_2O_3 nanoparticles without polymers were obtained and the particle size was about 340 nm (Fig. S4a, ESI†). When 30 μL of formaldehyde was added into the reaction system, γ-Fe_2O_3–polymer composites were formed

(Fig. S4b, ESI†). However, γ-Fe_2O_3 nanoparticles were incompletely wrapped in the polymer and the size was not uniform. Interestingly, when the volume of formaldehyde reached 50 μL, the γ-Fe_2O_3 nanoparticles in the composites were completely embedded in the polymers and the particle size was about 3.5 nm (Fig. S4c and S4d, ESI†). As the concentration of formaldehyde was increased, the polymer started to form and the γ-Fe_2O_3 nanoparticles in the polymer gradually became smaller as a result of the inhibition of growth of γ-Fe_2O_3 nanoparticles due to the presence of the polymers. When the concentration of formaldehyde solution was fixed, the influence of sodium hydroxide was investigated. When the volume of sodium hydroxide solution was increased from 0 to 350 μL, the polymer gradually formed and the size of γ-Fe_2O_3 nanoparticles gradually became smaller (Fig. S5, ESI†). The reasons were that the polymerization reaction needed to be undertaken under appropriate alkaline conditions, and the formation of the polymer also prevented the γ-Fe_2O_3 nanoparticles from growing further. Based on the results of control experiments, we believe that the formation of γ-Fe_2O_3–polymer composites is a result of the combined effects of formaldehyde and sodium hydroxide. In addition, we also proposed a possible synthetic mechanism (Fig. S6, ESI†). Iron(III) acetylacetonate decomposed under basic conditions to form iron hydroxide and an acetylacetonate anion (compound 1), of which the latter one formed an acetylacetonate carbanion (compound 2) as a result of the existing keto–enol tautomerization. The polymer was obtained through the aldol condensation reaction between the acetylacetonate carbanion and formaldehyde. This explained that the formation of polymers prevented the γ-Fe_2O_3 nanoparticles from growing further. To further verify the mechanism, we also replaced $Fe(acac)_3$ with $FeCl_3$ and acetylacetone. The TEM image (Fig. S7, ESI†) of the product shows that the sub-10 nm nanoparticles were wrapped in the polymer. The result is in agreement with the hypothesis of the mechanism.

The catalytic activity of the γ-Fe_2O_3–polymer composites for the reduction of nitrobenzene to aniline was evaluated at 85 °C in a round-bottomed flask (Fig. 3a). At the beginning of reaction, the yield of anilines increased with prolonged reaction time. After 20 min, the yield of anilines remained constant and was up to 100% (Fig. 3b). Even after nine cycles, γ-Fe_2O_3–polymer composites still had a good catalytic performance, while the yield of anilines was 88% (Fig. 3c) and the particle size of γ-Fe_2O_3 nanoparticles was still retained (Fig. S8, ESI†). The slight decrease of aniline yield after seven cycles was probably due to the loss of the catalyst in the transfer process. Compared to the yield in the reported literature[4] and yield obtained using commercial γ-Fe_2O_3, α-Fe_2O_3 and Fe_3O_4 (Table S2 and Fig. S9, ESI†), the composites showed a higher catalytic activity, which should be ascribed to the higher surface area of the porous composites and the smaller size of γ-Fe_2O_3 nanoparticles.[6] Meanwhile, the crystal phase also played a crucial role in catalytic activity. In addition, γ-Fe_2O_3–polymer composites also exhibited excellent catalytic performance when different nitroarenes were used as substrates (Table S3, ESI†). Therefore, the γ-Fe_2O_3–polymer composite catalyst can be applied in reducing different nitroarenes, which has potential applications in the catalytic industry.

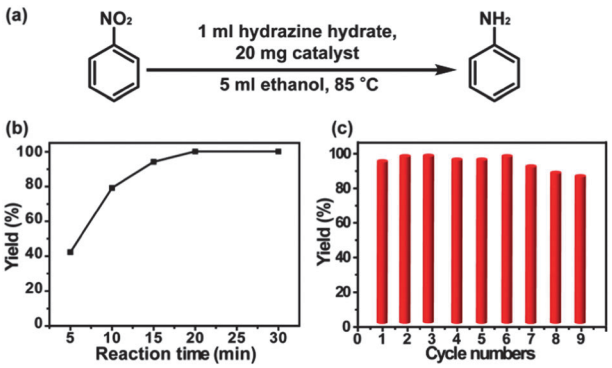

Fig. 3 (a) Reaction equation for the reduction of nitrobenzene to aniline. (b) The yield of aniline as a function of time. (c) Cycle performance test of the γ-Fe_2O_3–polymer composite catalyst for the reduction of nitrobenzene to aniline.

In summary, we have developed a facile one-pot approach for the synthesis of the γ-Fe_2O_3–polymer porous composites through the thermal decomposition of iron(III) acetylacetonate and formaldehyde under the alkaline conditions. The formed polymer inhibited the growth of the nanoparticles, and the average size of γ-Fe_2O_3 nanoparticles was 3.5 nm and these γ-Fe_2O_3 nanoparticles exhibited excellent catalytic activity and recyclability for the reduction of nitroarene to aminoarene. We believe that our synthetic strategy can be readily extended to the preparation of other metal oxide–polymer and metal–polymer composites with small particle size. Such composites will find many applications in catalysis, photovoltaics, and energy storage.

This work was supported by NSFC (No. 51001098, 21133010), the Institute of Metal Research (No. 09NBA211A1), MOST (No. 2011CBA00504), and the open project of State Key Laboratory of Urban Water Resource and Environment (No. QA201023). We acknowledge the help of Ms Yanjie Wang and Dr Xin Liu with the Mössbauer spectroscopy test and analysis.

Notes and references

1 I. Ali, *Chem. Rev.*, 2012, **112**, 5073.
2 L. Zhao, Y. F. Zhao and Y. Han, *Langmuir*, 2010, **26**, 11784.
3 X. L. Mou, B. S. Zhang, Y. Li, L. D. Yao, X. J. Wei, D. S. Su and W. J. Shen, *Angew. Chem., Int. Ed.*, 2012, **51**, 2989.
4 S. Kim, E. Kim and B. M. Kim, *Chem.–Asian J.*, 2011, **6**, 1921.
5 A. H. Lu, E. L. Salabas and F. Schüth, *Angew. Chem., Int. Ed.*, 2007, **46**, 1222.
6 X. L. Mou, X. J. Wei, Y. Li and W. J. Shen, *CrystEngComm*, 2012, **14**, 5107.
7 J. Rockenberger, E. C. Scher and A. P. Alivisatos, *J. Am. Chem. Soc.*, 1999, **121**, 11595.
8 G. Gao, P. Huang, Y. X. Zhang, K. Wang, W. Qin and D. X. Cui, *CrystEngComm*, 2011, **13**, 1782.
9 S. Laurent, D. Forge, M. Port, A. Roch, C. Robic, L. V. Elst and R. N. Muller, *Chem. Rev.*, 2008, **108**, 2064.
10 A. E. Kadib, K. Molvinger, C. Guimon, F. Quignard and D. Brunel, *Chem. Mater.*, 2008, **20**, 2198.
11 D. Kabra, M. H. Song, B. Wenger, R. H. Friend and H. J. Snaith, *Adv. Mater.*, 2008, **20**, 3447.
12 H. Zhang, Y. Liu, D. Yan and B. Yang, *Chem. Soc. Rev.*, 2012, **41**, 6066.
13 L. Machala, J. Tuček and R. Zbořil, *Chem. Mater.*, 2011, **23**, 3255.
14 M. J. Martínez-Pérez, R. de Miguel, C. Carbonera, M. Martínez-Júlvez, A. Lostao, C. Piquer, C. Gómez-Moreno, J. Bartolomé and F. Luis, *Nanotechnology*, 2010, **21**, 465707.
15 Z. Niu, J. Chen, H. H. Hng, J. Ma and X. Chen, *Adv. Mater.*, 2012, **24**, 4144.
16 D. Li, W. Y. Teoh, C. Selomulya, R. C. Woodward, P. Munroe and R. Amal, *J. Mater. Chem.*, 2007, **17**, 4876.
17 T. Fujii, F. M. F. de Groot, G. A. Sawatzky, F. C. Voogt, T. Hibma and K. Okada, *Phys. Rev. B*, 1999, **59**, 3195.
18 K. S. W. Sing, *Pure Appl. Chem.*, 1985, **57**, 603.

